

# Model-independent WIMP Characterisation using ISR

Christoph Bartels<sup>1</sup>, Olaf Kittel<sup>2</sup>, Ulrich Langenfeld<sup>3,\*</sup>, and Jenny List<sup>1 †</sup>

1- DESY, Notkestrasse 85, D-22607 Hamburg - Germany

2- Departamento de Física Teórica y del Cosmos and CAFPE,  
Universidad de Granada, E-18071 Granada, Spain

3- Institut für Theoretische Physik und Astronomie,  
Universität Würzburg, Am Hubland, D-97074 Würzburg, Germany

The prospects of measuring the parameters of WIMP dark matter in a model independent way at the International Linear Collider are investigated. The signal under study is direct WIMP pair production with associated initial state radiation  $e^+e^- \rightarrow \chi\chi\gamma$ . The analysis is performed in full simulation of the ILD detector concept. With an integrated luminosity of  $\mathcal{L} = 500 \text{ fb}^{-1}$  and realistic beam polarizations the helicity structure of the WIMP couplings to electrons can be determined, and the masses and cross sections can be measured to the percent level. The systematic uncertainties are dominated by the polarization measurement and the luminosity spectrum.

## 1 Radiative WIMP production in $e^+e^-$ collisions

New Weakly Interacting Massive Particles (WIMPs) with masses in the order of  $M_\chi \sim 100 \text{ GeV}$  are predicted by several extensions to the SM of particle physics. With their weak strength interactions, these particles are natural candidates for the observed abundance of cosmological Dark Matter (DM).

If these particles were produced at colliders, they would leave the detector invisibly without any further interaction. Their parameters could be inferred indirectly by the analysis of cascade decays if other new particles exist in the kinematically accessible mass range. Alternatively the direct pair production of WIMPs with associated initial state radiation  $e^+e^- \rightarrow \chi\chi\gamma$  can be employed to determine the WIMP properties from the observed photon spectrum. It has to be noted, that even if the detection via cascade decays is possible, the single photon plus missing energy signature provides an additional measurement of the WIMP candidate.

The rate of radiative WIMP production at an  $e^+e^-$  collider can be estimated model-independent without any assumptions on the dynamics of the interaction involved [1]. With only one new stable particle responsible for the observed DM content in the universe, the production cross section for WIMP pairs with associated ISR can be written in the limit of non-relativistic final state WIMPs as:

$$\frac{d\sigma}{dx d\cos\Theta} \approx \frac{\alpha\kappa_e\sigma_{\text{an}}}{16\pi} \frac{1+(1-x)^2}{x \sin^2\Theta} 2^{2J_0} (2S_\chi + 1)^2 \left(1 - \frac{4M_\chi^2}{(1-x)s}\right)^{1/2+J_0}, \quad (1)$$

with the candidate mass  $M_\chi$ , the candidate spin  $S_\chi$  and the center-of-mass energy squared  $s$ . The double differential cross section is expressed in the dimensionless variables  $x = \frac{2E_\gamma}{\sqrt{s}}$  and

---

\*U. L. has been supported by funding from the research training group GRK 1147 of the Deutsche Forschungsgemeinschaft and partially by the Helmholtz alliance 'Physics at the Terascale.

†The authors acknowledge the financial support of the Deutsche Forschungsgemeinschaft in the DFG project Li 1560/1-1.

$\Theta$  of the emitted photon. In Equation 1,  $J_0$  is the quantum number of the dominant partial wave in the production process. In the following, we will refer to the cases of  $J_0 = 0$  (s-wave) and  $J_0 = 1$  (p-wave) production only. The quantity  $\kappa_e$  is the “annihilation fraction” of WIMPs into electrons. The parameter  $\sigma_{an}$  provides the overall scale of the production cross section and can be inferred from observation when the WIMP is identified with the cosmological Dark Matter [1].

The annihilation fraction  $\kappa_e$  implicitly depends on the helicity of the initial state electrons. For our analysis we investigated the following three coupling scenarios [2]:

- **”Equal”**: The WIMP couplings are independent of the helicity of the incoming electrons and positrons, i.e.  $\kappa(e_R^-, e_L^+) = \kappa(e_R^-, e_R^+) = \kappa(e_L^-, e_L^+) = \kappa(e_L^-, e_R^+)$ .
- **”Helicity”**: The couplings conserve helicity and parity,  $\kappa(e_R^-, e_L^+) = \kappa(e_L^-, e_R^+)$ ;  $\kappa(e_R^-, e_R^+) = \kappa(e_L^-, e_L^+) = 0$ .
- **”Anti-SM”**: This scenario is a ”best case” scenario, since the WIMPs couple only to right-handed electrons and left-handed positrons:  $\kappa(e_R^-, e_L^+)$ .

This “single photon plus missing energy signature” has Standard Model (SM) processes with large cross sections for background, the dominant one being radiative neutrino production  $e^+e^- \rightarrow \nu\nu\gamma$ , which proceeds for high center-of-mass energies primarily via t-channel  $W$  exchange and hence is strongly polarisation dependent. In addition other SM processes like radiative Bhabha scattering  $e^+e^- \rightarrow e^+e^-\gamma$  or multi-photon final states can mimic the WIMP production signature when the accompanying electrons or photons leave the detector through the beam pipe, or are not properly reconstructed. Polarised beams can be used to significantly reduce these backgrounds and increase the S/B ratio [3], but the still large abundance of background events requires a consideration of systematic uncertainties from the detector measurement and beam parameters.

## 2 Data samples and event selection

To cover a broad range of parameters in terms of candidate masses, partial waves and coupling structures, only the SM background has been generated and simulated explicitly. The signal contribution to the data is obtained by reweighting the irreducible SM  $\nu\nu\gamma$  background, which is indistinguishable from the signal on an event-by-event basis, with the cross section ratio  $w_{sig}(E_\gamma) = \frac{d\sigma(\chi\chi\gamma)}{dE_\gamma} / \frac{d\sigma(\nu\nu\gamma)}{dE_\gamma}$  of radiative WIMP and neutrino pair production. The weights are evaluated in terms of the MC photon energy.

The measurement of the WIMP parameters requires a precise prediction of the SM background photon distributions. The expectation is generated by a parametrization of an independent background subsample, by successively correcting the SM prediction for the detector energy resolution and selection efficiencies. Remaining differences to the simulated detector output from the beam energy spectrum and unaccounted detector and reconstruction effects are parametrized with a higher order polynomial. From the parametrization of the  $\nu\nu\gamma$  spectra, the signal prediction is generated [2].

### 2.1 Simulation and reconstruction

The background events have been generated using WHIZARD [4]. The beam energy spectrum was provided by GUINEA PIG [5] for the nominal RDR baseline parameter set for a

$\sqrt{s} = 500$  GeV machine [6]. The simulation of the detector response was done for the ILD detector concept [7] with the GEANT4 [8] based simulation software MOKKA [9]. Three statistically independent event samples of  $\sim 50 \text{ fb}^{-1}$  each have been generated and simulated for the dominant irreducible  $\nu\nu\gamma$  background. The first two samples are used for the background and signal contribution to the data, while the third sample serves as basis for the spectrum parametrization. In addition data samples with multi-photon final states  $e^+e^- \rightarrow \gamma\gamma(N)\gamma$  and the Bhabha background  $e^+e^- \rightarrow e^+e^-\gamma$  have been simulated. After event reconstruction using the PANDORA PFA particle flow algorithm [10] two corrections to the reconstructed events have been applied. The reconstruction of high energy photons often results in several additional detections of lower energy photons, because the clustering stage of the PANDORA PFA algorithm tends to split large energy depositions into several smaller distinct electromagnetic clusters. To counter the effect of the cluster fracturing, photon candidates are merged with a cone based method. Second, the photon candidate energies have been recalibrated with a calibration function accounting for polar angle dependent fractional energy losses caused by the segmentation of the ILD calorimeter system.

## 2.2 Event selection

An event is considered signal-like, if it contains at least one high  $p_T$  photon with an energy between  $10 \text{ GeV} < E_\gamma < 220 \text{ GeV}$ , and a polar angle constrained to  $|\cos\Theta| < 0.98$ . The condition on the photon energy reduces the abundant low energy ISR from the SM background and excludes the massless neutrino final state on the radiative  $Z$  return at photon energies of  $E_\gamma \approx 241 \text{ GeV}$ . For further event selection, additional constraints are set to deal with the dominant reducible SM backgrounds, especially radiative Bhabha scattering and multi-photon final states. To exclude hadronic and leptonic final states, the maximal exclusive energy  $E_\gamma - E_{vis}$ , i.e. the full visible energy excluding the selected photon, is constrained to 20 GeV. For further reduction of hadronic final states and Bhabha events, the maximal allowed transverse track momentum is  $p_T < 3 \text{ GeV}$ . The track momenta can not be constrained stronger, as the event selection has to allow for tracks of  $e^+e^-$  pairs from the beamstrahlung background and for track overlays of multi-peripheral  $\gamma\gamma \rightarrow$  hadrons events (collectively called  $\gamma\gamma$  processes). In Figure 1(a) the momentum distribution of tracks per bunch crossing from the  $\gamma\gamma$  and beamstrahlung background are shown. On average 0.7 tracks from  $\gamma\gamma$  processes and 1.5 tracks from beamstrahlung are expected in each event. The distributions show a strong peak at low  $p_T$  determined from the minimal momentum for the tracks to reach the tracking region of ILD and fall off rapidly. Only 0.2% of tracks have a transverse momentum above 3 GeV. The selection efficiency of the  $\nu\nu\gamma$  background is on average above 85%, with higher efficiencies in the low energy part of the photon spectrum, where most of the WIMP production signal is located. This higher efficiency for low energies translates to a signal selection efficiency well above 90% over the full mass range, see Figure 1(b).

## 2.3 Systematic uncertainties

While the WIMP mass is predominantly determined from the polarisation independent threshold in the photon energy spectrum, the cross section determination requires a precise knowledge of the normalisation of the polarisation dependent  $\nu\nu\gamma$  background. The polarisation measurement precision is assumed to  $\delta P/P = 0.25\%$  [11]. The precision on

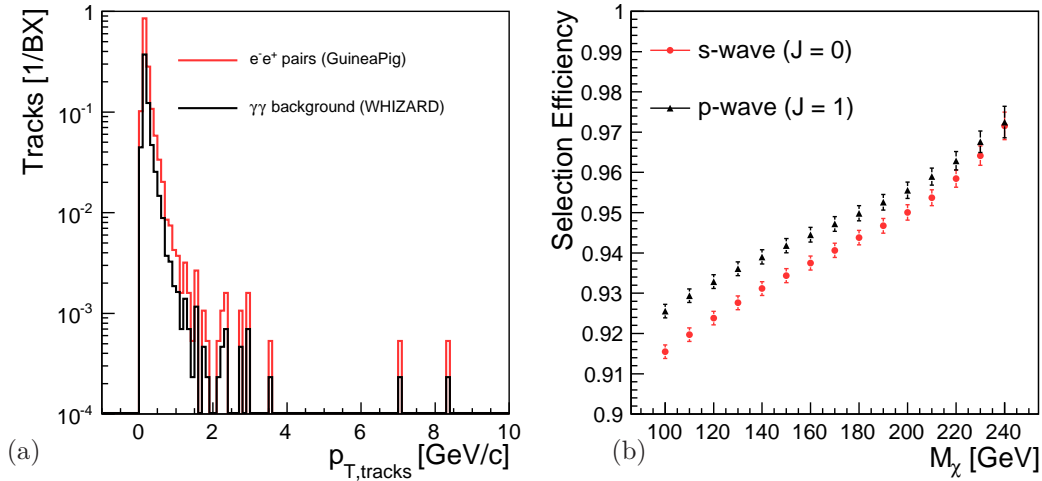


Figure 1: (a) Transverse momentum distribution of track overlays from the beamstrahlungs background (red/gray) and from  $\gamma\gamma$  processes (black). (b) Mass dependent signal selection efficiencies for s-wave (red/gray) and p-wave (black) WIMP production.

the luminosity is given by the RDR [6] with  $10^{-4}$ . A further source of systematic error is given by the knowledge of the beam energy spectrum. Here, its influence is conservatively estimated from the impact on the signal spectrum for two different parameter sets, namely the nominal RDR and SB-2009 [12] sets. For the cross section measurement which is not sensitive to the partial wave quantum number, the selection efficiency obtains an additional contribution of uncertainty from the difference between the selection efficiencies of s- and p-wave production.

### 3 Results

For the analysis a typical running scenario of the ILC is assumed, where an integrated luminosity of  $\mathcal{L} = 500 \text{ fb}^{-1}$  is distributed to four polarisation states with  $(+|P_{e-}|; -|P_{e+}|)$ ,  $(-|P_{e-}|; +|P_{e+}|)$ ,  $(+|P_{e-}|; +|P_{e+}|)$  and  $(-|P_{e-}|; -|P_{e+}|)$ . The odd (equal) sign configurations obtain 40% (10%) of the delivered luminosity each. The absolute polarization values are assumed to be  $|P_{e-}| = 0.8$  and  $|P_{e+}| = 0.3$  or  $|P_{e+}| = 0.6$ , respectively. The total unpolarised signal cross section in the signal region is set to  $\sigma_0 = 100 \text{ fb}$  throughout. For the determination of the cross section and coupling structure the candidate mass is fixed to 150 GeV.

#### 3.1 Helicity structure and cross section

With four different longitudinal polarization configurations, the fully polarized cross sections  $\sigma_{\{L,R\}}$ , and hence the helicity structure of the WIMP couplings to the beam electrons, can

be determined from the cross section deconstruction [3]

$$\begin{aligned} \sigma(P_{e^-}, P_{e^+}) = & \frac{1}{4} \left[ (1 + P_{e^-})(1 + P_{e^+})\sigma_{RR} + (1 - P_{e^-})(1 - P_{e^+})\sigma_{LL} \right. \\ & \left. + (1 + P_{e^-})(1 - P_{e^+})\sigma_{RL} + (1 - P_{e^-})(1 + P_{e^+})\sigma_{LR} \right]. \end{aligned} \quad (2)$$

	$( P_{e^-} ;  P_{e^+} ) = (0.8; 0.3)$		$( P_{e^-} ;  P_{e^+} ) = (0.8; 0.6)$	
<b>"Helicity"</b> scenario				
$\sigma_{RL}/\sigma_0$	$1.99 \pm 0.24$	(0.16)	$1.99 \pm 0.10$	(0.08)
$\sigma_{RR}/\sigma_0$	$0.00 \pm 0.33$	(0.21)	$0.00 \pm 0.23$	(0.14)
$\sigma_{LL}/\sigma_0$	$0.00 \pm 0.37$	(0.29)	$0.00 \pm 0.23$	(0.15)
$\sigma_{LR}/\sigma_0$	$1.95 \pm 0.38$	(0.25)	$1.95 \pm 0.29$	(0.16)

Table 1: Fully polarized cross sections  $\sigma_{\{R,L\}}$  measured within the **"Helicity"** WIMP scenario and for two different absolute polarizations of electrons and positrons. The quoted uncertainties are the squared sum of statistical errors and systematic uncertainties, with the bracketed values corresponding to an increased precision on the polarization measurement of  $\delta P/P = 0.1\%$ .

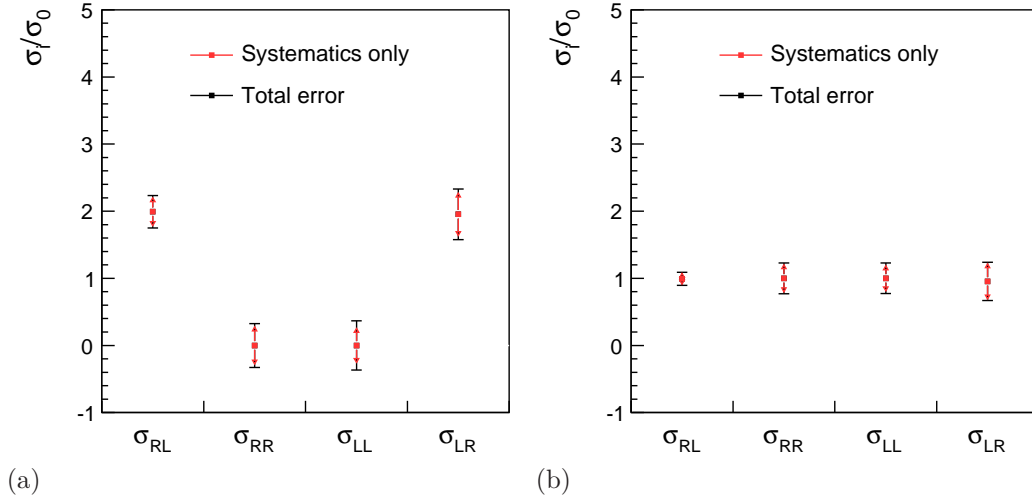


Figure 2: Helicity structure of WIMP couplings in terms of the fully polarised cross sections  $\sigma_{\{R,L\}}$  in (a) the **"Helicity"** scenario and (b) the **"Equal"** scenario. The values are normalised to the unpolarised cross section  $\sigma_0$ .

The results for the **"Helicity"** coupling scenario are listed in terms of the fully polarized cross sections  $\sigma_{\{R,L\}}$  in Table 1 and shown in Figure 2(a). Figure 2(b) depicts the measurement in the **"Equal"** scenario. Given the input cross section of 100 fb, the fully polarized cross sections can be determined to 20 fb to 40 fb with a positron polarization of 30%. The uncertainties are reduced to 10 to 30 fb with an increased positron polarization

of 60%. This is in particular the case for  $\sigma_{\{L,R\}}$ , which is primarily determined by the measurement  $\sigma_{+-}$  with positive electron and negative positron polarization. In that case the SM background is maximally reduced. The dominant source of systematic uncertainty stems from the polarization measurement.

Assuming uncorrelated polarisation errors, a combination of the four individual measurements provides a determination of the unpolarised cross section  $\sigma_0$  to a precision of 3 to 5% for an positron polarisation of  $P = 30\%$ , depending on the coupling scenario, see Table 2. With an increased positron polarisation of  $P = 60\%$ , the relative precision is increased to 2.5%. Again the dominant source of systematic uncertainty comes from the polarization measurement.

Data scenario	Unpolarized cross section: $\sigma_0 \pm \text{stat} \pm \text{sys} (\pm \text{total})$ [fb]			
(simulated)	$( P_{e-} ;  P_{e+} ) = (0.8; 0.3)$		$( P_{e-} ;  P_{e+} ) = (0.8; 0.6)$	
Assumed polarization uncertainty	$\delta P/P = 0.25\%$			
<b>"Equal"</b>	$99.0 \pm 2.8 \pm 4.3$	$(\pm 5.1)$	$99.2 \pm 2.7 \pm 3.5$	$(\pm 4.4)$
<b>"Helicity"</b>	$99.1 \pm 2.3 \pm 4.0$	$(\pm 4.6)$	$99.4 \pm 2.0 \pm 2.8$	$(\pm 3.4)$
<b>"Anti-SM"</b>	$99.8 \pm 1.4 \pm 2.8$	$(\pm 3.2)$	$99.7 \pm 1.1 \pm 2.1$	$(\pm 2.4)$

Table 2: Measured unpolarized cross section  $\sigma_0$  by a combination of cross section measurements with polarized beams for an integrated luminosity of  $\mathcal{L} = 500 \text{ fb}^{-1}$ .

### 3.2 Mass measurement and partial wave

The candidate mass is measured by fitting template spectra for s+b to the measured data spectrum. The mass is determined by the  $\chi^2$  of the measurement. Depending on the coupling scenario, polarization configuration, the candidate mass can be determined to a level of  $< 2\%$ , see Table 3.

Mass [GeV]	WIMP mass: $\pm \text{stat.} \pm \delta E (\text{sys.}) \pm \delta \mathcal{L} (\text{sys.})$ (total) [GeV]					
	$(P_{e-}; P_{e+}) = (0.8; 0.0)$		$(P_{e-}; P_{e+}) = (0.8; -0.3)$		$(P_{e-}; P_{e+}) = (0.8; -0.6)$	
<b>"Helicity"</b> scenario						
120	$2.67 \pm 0.07 \pm 1.91$	$(3.29)$	$1.92 \pm 0.07 \pm 1.89$	$(2.70)$	$1.53 \pm 0.07 \pm 1.89$	$(2.43)$
150	$2.11 \pm 0.05 \pm 1.47$	$(2.57)$	$1.62 \pm 0.05 \pm 1.46$	$(2.18)$	$1.23 \pm 0.05 \pm 1.45$	$(1.90)$
180	$1.78 \pm 0.03 \pm 1.00$	$(2.04)$	$1.36 \pm 0.03 \pm 1.00$	$(1.69)$	$0.94 \pm 0.03 \pm 1.00$	$(1.37)$
210	$0.78 \pm 0.02 \pm 0.54$	$(0.95)$	$0.67 \pm 0.02 \pm 0.54$	$(0.87)$	$0.59 \pm 0.02 \pm 0.54$	$(0.80)$

Table 3: Statistical and systematic uncertainties on the measured WIMP masses for an integrated luminosity of  $\mathcal{L} = 500 \text{ fb}^{-1}$  in the **"Helicity"** coupling scenarios for three different polarization configurations.

The dominant source of systematic uncertainty come from the calibration of the overall energy scale ( $\delta E$ ) and the measurement of the beam energy spectrum ( $\delta \mathcal{L}$ ).

An indication of the dominant partial wave in the production process is obtained from the  $\chi^2$  value of fitting s- and p-wave template spectra against the data spectrum. In all

studied scenarios the fit converges better for the correct partial wave assumption. However, with unpolarised beams, the distinction is not very clear over the full mass range. Utilising the possibility of polarised positrons allows to clearly separate the s- and p-wave production.

## References

- [1] A. Birkedal, K. Matchev, M. Perelstein, Phys. Rev. **D70** (2004) 077701. [hep-ph/0403004].
- [2] C. Bartels, Diploma Thesis, C. Bartels, PhD Thesis, DESY-THESIS-2011-034.
- [3] G. Moortgat-Pick *et al.*, Phys. Rept. **460**, 131 (2008) [arXiv:hep-ph/0507011].
- [4] W. Kilian, T. Ohl and J. Reuter, Eur. Phys. J. C **71** (2011) 1742 [arXiv:0708.4233 [hep-ph]].
- [5] D. Schulte, TESLA 97-08 (1996).
- [6] N. Phinney, ICFA Beam Dyn. Newslett. **42** (2007) 7.
- [7] T. Abe *et al.* [ILD Concept Group - Linear Collider Collaboration], arXiv:1006.3396 [hep-ex].
- [8] S. Agostinelli *et al.* [GEANT4 Collaboration], Nucl. Instrum. Meth. A **506**, 250 (2003).
- [9] MOKKA, <http://polzope.in2p3.fr:8081/MOKKA>
- [10] M. A. Thomson, Nucl. Instrum. Meth. A **611** (2009) 25 [arXiv:0907.3577 [physics.ins-det]].
- [11] S. Boogert *et al.*, JINST **4** (2009) P10015. [arXiv:0904.0122v2 physics.ins-det].
- [12] M. Berggren, arXiv:1007.3019 [hep-ex].